International Journal of Pharmaceutics 413 (2011) 229–236

Contents lists available at ScienceDirect

International Journal of Pharmaceutics

journal homepage: www.elsevier.com/locate/ijpharm

Pharmaceutical Nanotechnology

Chitosan/sulfobutylether-β-cyclodextrin nanoparticles as a potential approach for ocular drug delivery

Azza A. Mahmoud [a,*], Gina S. El-Feky [a], Rabab Kamel [a], Ghada E.A. Awad [b]

[a] Pharmaceutical Technology Department, National Research Center, Dokki, Tahreer St., Cairo, Egypt
[b] Chemistry of Natural and Microbial Product Department, National Research Center, Dokki, Cairo, Egypt

ARTICLE INFO

Article history:
Received 17 February 2011
Received in revised form 10 April 2011
Accepted 14 April 2011
Available online 21 April 2011

Keywords:
Nanoparticles
Chitosan
Sulfobutylether-β-cyclodextrin
Ocular
Zeta potential
Mucoadhesion

ABSTRACT

Development of efficient ocular delivery nanosystems remains a major challenge to achieve sustained therapeutic effect. The purpose of this work was to develop chitosan nanoparticles using sulfobutylether-β-cyclodextrin (SBE-β-CD) as polyanionic crosslinker and to investigate the potential of using those nanostructures as ocular drug delivery systems. Econazole nitrate (ECO) was chosen as model drug molecule. The influence of different process variables (chitosan molecular weight and the concentration of the two ionic agents) on particle size, polydispersity index, zeta potential, drug content, *in vitro* release and mucoadhesive properties was investigated. The results showed that the prepared nanoparticles were predominant spherical in shape having average particle diameter from 90 to 673 nm with positive zeta potential values from 22 to 33 mV and drug content values ranging from 13 to 45%. Drug release from optimized nanoparticles was controlled with approximately 50% of the original amount released over a 8 h period. The release profile of nanoparticles followed a zero-order release kinetics. The optimized nanoparticles were tested for their use as ocular drug delivery systems on albino rabbits. The *in vivo* studies revealed that the prepared mucoadhesive nanoparticles had better ability in sustaining the antifungal effect of ECO than the ECO solution. Therefore, chitosan/SBE-β-CD nanoparticles developed showed a promising carrier for controlled delivery of drug to the eye.

1. Introduction

The use of nanotechnology provides attractive opportunities for ocular drug delivery, mainly because the association of an active molecule to a nanocarrier allows the molecule to interact intimately with specific ocular structures and thus overcome ocular barriers and prolong its residence in the target tissue (de la Fuente et al., 2010). Furthermore, this technology offers promising solution for formulating various poorly water soluble drugs in the form of eye drops (Kayser et al., 2005).

The short residence time of colloidal systems in the ocular mucosa is main problem in the therapy of ocular diseases. Since the cornea and conjunctiva have a negative charge, it was thought that the use of mucoadhesive polymers would increase the residence time of the associated drug interaction these extraocular structures (De Campos et al., 2001). Chitosan (CS) is a natural cationic polyelectrolyte polymer obtained by the deacetylation of chitin. CS is a non-toxic, biocompatible and biodegradable polysaccharide (Paul and Sharma, 2000) in addition to its favourable mucoadhesiveness and ability to increase the membrane permeability (Colonna et al., 2008). More importantly, CS nanoparticles can be spontaneously formed through ionic gelation using a negatively charged compound as precipitating agent, so that the use of harmful organic solvents can be avoided during preparation and loading (van der Lubben et al., 2001).

Cyclodextrins (CDs) are cyclic oligosaccharides with a hydrophilic exterior surface and a hydrophobic interior cavity. As such, they can interact with molecules of small size to form total inclusion complexes, or with macromolecular drugs to form partial inclusion complexes through their hydrophobic side chains (Aachmann et al., 2003). One of the most prominent groups of modified CDs are the sulfobutyl-substituted CDs, among which is the sulfobutylether-β-cyclodextrin (SBE-β-CD). SBE-β-CD is a polyanionic CD derivative, with an average degree of substitution of seven and has much greater solubility in water than the parent β-CD. The inclusion ability of SBE-β-CD is generally greater than that of β-CD due to the hydrophobic butyl side arms that extend from the hydrophobic cavity of the CD (Zia et al., 2001). The unique properties of SBE-β-CD (being polyanionic and solubilizing agent) makes it a versatile substance, which can form nanoparticles with CS by ionic gelatin and in addition to solubilization of poorly water soluble drugs.

Econazole nitrate (ECO) is an imidazole antifungal agent largely used for the treatment of many mycotic infections of skin, hair

* Corresponding author. Tel.: +20 103061120; fax: +20 233370931.
E-mail address: azzaamahmoud@yahoo.com (A.A. Mahmoud).

0378-5173/$ – see front matter © 2011 Elsevier B.V. All rights reserved.
doi:10.1016/j.ijpharm.2011.04.031

and mucous membranes (Reynolds, 1996). However, the poor aqueous solubility of this drug has discourage its use for the treatment of ophthalmic fungal infection (Al-Marzouqi et al., 2009). Therefore, it is desirable to formulate ECO in a suitable system that could deliver it in an efficient concentration to the eye as chitosan nanoparticles. It is expected for ECO to form a complex with SBE-β-CD in the chitosan/SBE-β-CD nanoparticles. The mode of interaction is presumed to be hydrophobic interaction with the cavity interior along with additional charge–charge interaction between the cationic charged ECO and anionic charged SBE-β-CD (Zia et al., 2001).

The aim of this study was to adapt the ionic gelation technique for the encapsulation of ECO as a model drug into CS nanoparticles and to evaluate their potential as drug nanocarriers. We intended to combine the advantages of the mucoadhesive cationic CS nanocarriers and of the anionic SBE-β-CD in one delivery system for the sustained delivery of ECO to the eye. The CS nanoparticles prepared *via* the ionic gelation method were optimized by studying the influence of several key parameters including CS concentration and molecular weight (150 kDa *vs.* 360 kDa), CS/SBE-β-CD ratio and drug loading. The resulting nanoparticles were evaluated for their shape, drug content, process yield, size, zeta potential and drug release. The physicochemical characteristics of selected nanoparticles were examined by Fourier transform infrared spectroscopy (FT-IR), X-ray diffraction (XRD) and differential scanning calorimetry (DSC). Selected ECO nanoparticles were tested for their antifungal activity *in vivo* in rabbits eye and compared to that of drug solution.

2. Materials and methods

2.1. Materials

Econazole nitrate (ECO) was obtained from Erregierre SpA, Italy. Low viscosity chitosan (LMwt CS; 150 kDa), high viscosity chitosan (HMwt CS; 360 kDa) and porcine mucin were purchased from Sigma–Aldrich Chemie GmbH, Japan. Sulfobutylether-β-cyclodextrin sodium salt (SBE-β-CD, MW 2160) was kindly provided by Cydex L.C., USA. Dialysis tubing cellulose membrane (molecular weight cut-off 12,000 g/mole) was purchased from Sigma Chemical Company, USA. Glacial acetic acid was obtained from El Nasr Pharmaceutical Chemicals, Egypt. Potassium dihydrogen phosphate and disodium hydrogen phosphate were purchased from Sisco Research Laboratories Pvt. Ltd., India.

2.2. Methods

2.2.1. Investigating the conditions for CS nanoparticles formulation

CS nanoparticles were prepared using the method developed by Calvo et al. (1997) with modification based on the ionotropic gelation of CS with SBE-β-CD. Preliminary experiments were done to determine the formation nanoparticles zone. CS or SBE-β-CD were dissolved in pH 4 acetic acid aqueous solution in various concentrations. Then, SBE-β-CD solution was added to CS solution in a ratio of 1:3 (v/v) through a syringe needle under magnetic stirring at room temperature. The final concentrations of CS in the preparation were from 0.05 to 0.25% (w/w) and for SBE-β-CD were from 1.0 to 3.5% (w/w). Then samples were visually analysed and three different systems were identified and represented in a phase diagram: clear solution, opalescent suspension and aggregates. The aggregates were primary demonstrated as a suspension that was then quickly sediment after few minutes and thus a decrease in turbidity was observed.

2.2.2. Characterization of the nanoparticles

2.2.2.1. Nanoparticles size and zeta potential. The average particle size, size distribution (polydispersity index; PDI) and the zeta potential of the nanoparticles were analysed by photon correlation spectroscopy and laser Doppler anemometry, respectively, using a Zetasizer Nano ZS (Malvern Instruments, UK). Prepared nanoparticles were separated and subjected to measurement following dilution with 0.45 μm filtered distilled water. Particle size and PDI measurements were performed at a scattering angle of 90° and at a temperature of 25 °C. The hydrodynamic diameter was calculated from the autocorrelation function of the intensity of light scattered from particles with the assumption that the particles had a spherical form. The samples for zeta potential were placed in a disposable zeta cell at a temperature of 25 °C and were measured using PALS technology.

2.2.2.2. Nanoparticles morphology. The morphological examination of the nanoparticles was performed by transmission electron microscopy (TEM) (Jeol, JEM-1230, Japan). The nanoparticles were applied to a carbon-coated 300 copper grid and then were stained with 2% phosphotungstic acid for viewing by TEM.

2.2.2.3. Econazole nitrate (ECO) loaded nanoparticles. Selected nanoparticles area from the previous study was prepared in the presence of ECO in the SBE-β-CD solution with a final concentration of 1 mg/ml. The drug content of nanoparticles was determined by the separation of drug-loaded nanoparticles from the aqueous medium containing non-associated ECO by cooling centrifugation (Union 32R, Hanil Science Industrial Co., Korea) at 9,000 rpm and −5 °C for 30 min. The nanoparticles were mixed with 0.1 N HCl and sonicated for 10 min to obtain a clear solution. The concentration of ECO in 0.1 N HCl was determined spectrophotometrically by measuring the UV absorbance at 270.5 nm (Shimadzu UV spectrophotometer, 2401/PC, Japan).

The actual yield of CS nanoparticles from 100 ml of preparations was weight and presented. The ECO content, loading capacity of the nanoparticles and process yield were calculated as follows:

$$\text{Drug content (\%)} = \frac{\text{Amount of encapsulated drug}}{\text{Total amount of ECO}} \times 100.$$

$$\text{Loading capacity (\%)} = \frac{\text{Amount of encapsulated drug}}{\text{Weight of nanoparticles}} \times 100.$$

$$\text{Yield (\%)} = \frac{\text{Nanoparticles weight}}{\text{Weight of total components}} \times 100.$$

2.2.2.4. In vitro release studies. The release of ECO from CS nanoparticles was studied by dialysis method in pH 7.4 phosphate buffer. The prepared nanoparticles were separated from the aqueous medium containing non-associated ECO by cooling centrifugation (Union 32R, Hanil Science Industrial Co., Korea) at 9,000 rpm and −5 °C for 30 min and resuspended in phosphate buffer pH 7.4. Nanoparticles (equivalent to 1 mg of drug) were instilled in the dialysis bag which was secured with two clamps at each end. The dialysis bag was dipped into the receptor compartment containing 50 ml of the dissolution medium stirred continuously at 100 rpm and maintained at 37 °C. The receptor compartment was closed to prevent evaporation of the dissolution medium. Samples were withdrawn at regular time intervals, and the same volume was replaced with fresh dissolution medium. The samples were spectrophotometrically measured at 218 nm (Shimadzu UV spectrophotometer, 2401/PC, Japan).

The different release kinetics are assumed to reflect different release mechanisms. Therefore, three kinetic models including the

zero-order release equation, Higuchi equation and first-order equation were applied to process the *in vitro* data to find the equation with the best fit.

In addition, the similarity factor f_2 (U.S. Department of Health and Human Services, 1997) was used to compare the difference of dissolution profiles between the tested formulations. f_2 values greater than 50 (50–100) represent equivalence of the two curves.

2.2.2.5. Fourier transform infrared spectroscopy (FT-IR). FT-IR spectra for ECO, CS, SBE-β-CD, physical mixture and CS nanoparticles were monitored as KBr disc using a Shimadzu 435 U-O4 IR spectrophotometer, Japan. The characteristic peaks were recorded for different samples.

2.2.2.6. Differential scanning calorimetry (DSC). DSC analysis for ECO, CS, SBE-β-CD, physical mixture and CS nanoparticles were performed using a Shimadzu differential scanning calorimeter (DSC-50, Shimadzu, Japan). The apparatus was calibrated with purified indium (99.9%). Samples were placed in flat-bottomed aluminum pan and heated at a constant rate of 10 °C/min in an atmosphere of nitrogen in a temperature range of 20–500 °C.

2.2.2.7. X-ray diffractometry. X-ray diffraction patterns for ECO, CS, SBE-β-CD, physical mixture and CS nanoparticles were obtained by using a Diano X-ray diffractometer equipped with Cu Kα. The tube was operated at 45 kV, 9 mA.

2.2.2.8. Mucoadhesion studies. Equal volumes of mucin solution (0.4 mg/ml) and CS nanoparticles were vortexed for 1 min and the zeta potential of the mixtures was measured by Zetasizer Nano ZS (Malvern Instruments Ltd., UK).

2.2.3. In vivo evaluation of ECO-CS nanoparticles

2.2.3.1. Microbiological assays. Candida albicans (C. albicans) susceptibility to ECO. C. albicans NRRL Y-477 was chosen as a test organism for ECO. Test tubes containing 5 ml of Sabourand dextrose broth (Sbb) were inoculated with 100 μl of yeast suspension containing 1×10^8 CFU/ml.

Animals. Age matched male albino rabbits weighing 1.5–2.0 kg were used in this study. The animals were housed in individual cages in an air-conditioned room with free access to food and water. The artificial fluorescent light provided a cycle of night and day, 12 h each at 25 ± 0.5 °C and fed a standard pellet diet and water. All animals were healthy and free of clinically observed abnormalities. The studies conducted in full compliance with local, national, ethical and regulatory principles for animal care and were approved by the National Research Centre Ethics and Animal Care Committee.

2.2.3.2. Susceptibility test. The chitosan and SBE-β-CD solutions used for the nanoparticles formlations were sterilized by filtration through sterile 0.22 μm pore size pyrogen-free cellulose filters and the nanoparticles preparation process was done under aseptic conditions

The *in vivo* test was carried out for the prepared ECO loaded CS nanoparticles LC3-2 and LC5 as well as ECO solution (0.2%). The ECO loaded CS nanoparticles were dispersed in phosphate buffer solution (pH 7.4) to obtain 0.2% ECO concentration. Sterile 6 mm diameter filter paper discs (Watman no. 1) were placed under the eyelid of rabbit for 1 min at specific time intervals (1, 2, 3, 4, 5, 6, 7 and 8 h) following a single installation of the investigated formulae (50 μl) each in the conjunctival sac of the right eyes of six rabbits. The discs were then placed in the inoculated Sbb tubes. Then, the inoculated broth was incubated at 27 ± 0.5 °C for 24 h. The growth inhibition of yeast was evaluated by measuring the cultures' optical density at 600 nm using Shimadzu UV spectrophotometer, 2401/PC, Japan. Percent inhibition, which relates to the level of ECO in the eye tears following the topical application of tested ECO formulae, was calculated using Sbb medium inoculated with *C. albicans* NRRL Y-477 as control. The area under the curve from 1 to 8 h (AUC_{1-8}) was estimated by the linear trapezoidal method and used to predict and compare the mean time for the antifungal effect of ECO in the eye tears obtained from the tested ECO loaded CS nanoparticles as well as ECO solution.

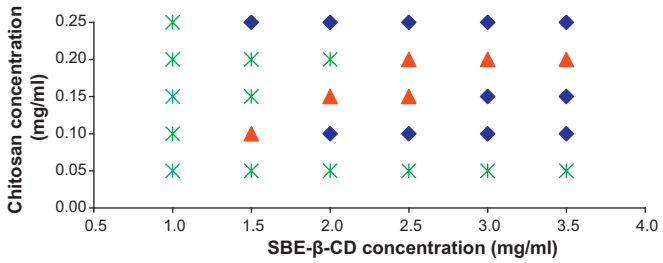

Fig. 1. . Phase diagram of nanoparticle formation for LMwt CS/SBE-β-CD with three areas: clear solution (✳); opalescent dispersion (▲); aggregates (◆). (For interpretation of the references to color in this figure legend, the reader is referred to the web version of the article.)

2.2.3.3. Statistical analysis. Pairs of groups were compared by performing one-tailed Student's *t*-test and multiple group comparison was conducted by one-way analysis of variance (ANOVA) and then by LSD using statistical software (SPSS, Chicago). All data are presented as a mean value with its standard deviation indicated (mean ± SD). *p*-Values less than 0.05 were considered to be statistically significant.

3. Results and discussion

3.1. Investigating the conditions for CS nanoparticles formulation

The ratio between CS and SBE-β-CD is critical and controls the size of the prepared particles. For this reason before the drug encapsulation into CS nanoparticles, it was necessary to establish the best ratio between components that enabled formation of the nanosystems.

Different concentrations of CS and SBE-β-CD were used to establish preparation conditions at which nanoparticles are formed. Three different systems were identified in the studied phase diagram: clear solution, opalescent dispersion and aggregates (Figs. 1 and 2). In general, it is possible to argue that when the amount of SBE-β-CD was too low (relative to CS), nanoparticles could not be formed, or that the quantity of the formed nanoparticles was too low. Nanoparticles with different characteristics were obtained when optimum amounts of CS and SBE-β-CD were used. However, increasing CS concentration as well as increasing SBE-β-CD concentration leads to an increase in particle diameters and to

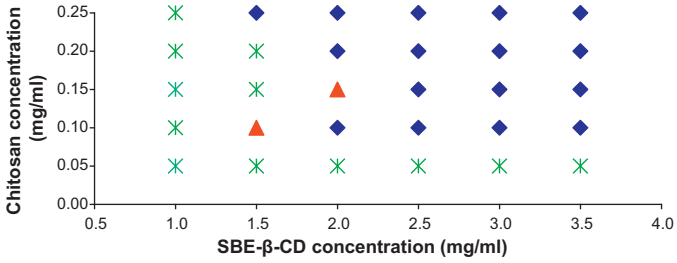

Fig. 2. Phase diagram of nanoparticle formation for HMwt CS/SBE-β-CD with three areas: clear solution (✳); opalescent dispersion (▲); aggregates (◆). (For interpretation of the references to color in this figure legend, the reader is referred to the web version of the article.)

agglomeration of the produced particles. This might be due to that when the amount of SBE-β-CD is high, an increase in the shielding of free positively charged groups of CS occurs which cause a decrease in the positive zeta potential values for the nanoparticles. This decrease in the positive zeta potential values cause a reduction in the repulsive forces between the nanoparticles and thus cross-bridge formation between nanoparticles occurs resulting in agglomeration of the nanoparticles (Cui et al., 2006; Oyarzun-Ampuero et al., 2009).

The effect of the molecular weight of the used CS had an impact on nanoparticle formation. It was found that using LMwt CS resulted in the formation of larger nanoparticle area compared to the use of HMwt CS. This can be explained by the decrease in viscosity as the molecular weight of CS decreases and the simultaneous increase in the ability of LMW CS to form smaller structures (Csaba et al., 2009).

CS/SBE-β-CD ratios that led to formation of opalescent suspension were selected for the preparation of drug-loaded nanoparticles (Table 1).

3.2. Characterization of the nanoparticles

3.2.1. Nanoparticles size and zeta potential

The reduced sizes of the NP formulations are very interesting in view of their potential application in ocular drops formulations. Indeed, it is well known that particles in the nanometric range are easily transported more efficiently through biological barriers (Csaba et al., 2006) and, therefore, the reduction achieved in particle size could result in more efficient drug delivery. All the resulting nanosystems ranged in diameter from 90.8 to 461.2 nm with a polydispersity index values between 0.16 and 0.64 (Table 1).

The effect of CS and SBE-β-CD concentration on the mean nanoparticle diameter were examined. The nanoparticles diameter appears to be dependent on the concentration of the two cross-linking agents (CS and SBE-β-CD), the minimum diameter, i.e. 90.8 nm, corresponding to the lowest CS and SBE-β-CD concentration (formula LC1) and the maximum diameter, i.e. 461.2 nm, corresponding to the highest CS and SBE-β-CD concentrations (formula LC6). Increasing the concentration of CS from 0.15 mg/ml for formula LC3 to 0.2 mg/ml for formula LC4 at a constant SBE-β-CD concentration (2.5 mg/ml), showed a significant increase ($p < 0.05$) in the particle diameter from 182.3 to 198.1 nm, respectively. The increased particles diameters were attributed to the increase in CS viscosity (Kawashima et al., 2000) and the higher availability of protonated amine groups for ionic gelation with increasing CS concentration (Motwani et al., 2008). Also, increasing the concentration of SBE-β-CD from 2.5 and 3.0 mg/ml for formula LC4 and LC5, respectively, to 3.5 mg/ml for formula LC6 at a constant CS concentration (0.2 mg/ml), showed a greatly increase ($p < 0.05$) in the particle diameter from 198.1 and 185.1 to 461.2 nm, respectively. The increased diameters of nanoparticles, could be due to slight aggregation caused by the reduction of surface positive charge resulting in reducing the repulsion forces between particles (Cui et al., 2006).

The polydispersity index (PDI) is a factor that represents the dispersion homogeneity. The PDI for all the formulations (except LC6) was found to be smaller than 0.4 that indicate a relative homogeneous dispersion (Table 1). The reason of broad size distribution for LC6 possibly due to aggregation of CS nanoparticles.

Zeta potential studies of the nanoparticles showed values ranging from +24.4 to +33.5 mV (Table 1). These positive zeta potential values indicate that the surface of the nanosystems is mostly composed by CS (Oyarzun-Ampuero et al., 2009). This net positive charge of the particles is desirable to prevent particle aggregation and promote electrostatic interaction with the overall negative charge of the cell membrane (Schiffelers et al., 2004). In general, it was noted that the zeta potential of nanoparticles decrease as CS/SBE-β-CD ratios decreased. The lower zeta potential with increasing SBE-β-CD amounts might be caused by an increased masking of free positively charged amino groups of CS (Krauland and Alonso, 2007). In addition, increasing CS concentration resulted in an increase in the nanoparticles zeta potential due to increasing of free positively charged amino groups of CS. The zeta potential of nanoparticles was not significantly modified ($p > 0.05$) by the CS molecular weight.

3.2.2. Nanoparticles drug content, loading capacity and process yield

Table 2 shows the nanoparticles drug content, loading capacity, actual yield and process yield. The nanoparticles drug content ranged between 13.37 and 45.67% depending on the CS to SBE-β-CD concentration used. The process yield values for the prepared nanoparticles ranged from 22.03 to 37.03%. The nanoparticles prepared using HMwt CS showed lower ($p < 0.05$) nanoparticles drug content and loading capacity values compared to those prepared using LMwt CS. It was reported that the high viscous nature of the gelation medium hinders the encapsulation of drug in a study on chitosan–alginate microspheres (Vandenberg et al., 2001). In addition, increasing the concentration of CS from 0.15 mg/ml for formula LC3 to 0.2 mg/ml for formula LC4 at a constant SBE-β-CD concentration (2.5 mg/ml), showed a significant decrease ($p < 0.05$) in the drug content from 41.51 to 35.41%, respectively. This indicates that relatively lower viscosity of the lower CS concentration promotes the interaction between CS and SBE-β-CD.

It can be observed that the drug content of the nanoparticles depended upon the concentration of the two cross linking ionic agents (CS and SBE-β-CD), the minimum value, i.e. 23.97%, corresponding to the lowest CS and SBE-β-CD concentration (formula LC1) and the maximum value, i.e. 45.67%, corresponding to the highest CS and SBE-β-CD concentrations (formula LC6). This is attributed to the increase in the amount of formed nanoparticles (indicated by the high actual yield value) due to the greater concentration of the two cross linking agents (CS and SBE-β-CD) available to form nanoparticles and thus to encapsulate the drug.

The prepared nanoparticles that showed significantly high drug content ($p < 0.05$), namely LC3, LC5 and LC6, were chosen for further optimization. The loaded drug was increased in the preparation medium from 1 mg/ml to 2 and 3 mg/ml. LC3-2, LC5-2 and LC6-2 were prepared with drug loading of 2 mg/ml, while LC3-3, LC5-3 and LC6-3 were prepared with drug loading of 3 mg/ml. The zeta potential values did not appear to be correlate to the initial ECO concentration in the SBE-β-CD solution (Table 3).

The nanoparticles drug content values were affected by the initial ECO concentration in the SBE-β-CD solution (Table 3). The increase in ECO concentration led generally to a decrease in nanoparticles drug content values, whereas an enhancement of loading capacity was observed. This could be explained by the fact that lower drug to polymers weight ratio, many drug molecules are adsorbed on the surface of nanoparticles; at higher drug to polymer weight ratio, nanoparticles surfaces became almost saturated with drug. Thus, there were only few drug molecules adsorbed onto the surfaces of nanoparticles. Therefore, the drug content values of the nanoparticles decreased with the increase of weight ratio of drug to polymer.

A correlation can be observed between the particle diameter and drug content in the same nanoparticle formula (LC3, LC5 or LC6) where by decreasing the drug content value a decrease in the particle diameter was observed except for LC6-2. A possible explanation may be that decreasing the encapsulated drug in the nanoparticles may led to a more compact solid matrix structure due to increasing CS/SBE-β-CD interaction, leading to decreasing nanoparticles size.

Table 1
Effect of chitosan concentration, molecular weight and SBE-β-CD concentration on the particle diameter, polydispersity index (PDI) and zeta potential for the prepared nanoparticles (mean ± SD).

Formula code	HMwt CS mg/ml	LMwt CS mg/ml	SBE-β-CD mg/ml	Particle diameter (nm)	PDI	Zeta potential (mV)
HC1	0.10		1.5	115.60 ± 18.30	0.217 ± 0.020	+25.1 ± 3.0
HC2	0.15		2.0	132.20 ± 10.50	0.164 ± 0.022	+27.1 ± 2.6
LC1		0.10	1.5	90.81 ± 8.10	0.215 ± 0.025	+24.4 ± 2.8
LC2		0.15	2.0	181.10 ± 12.50	0.259 ± 0.026	+31.3 ± 3.6
LC3		0.15	2.5	182.30 ± 10.30	0.353 ± 0.031	+25.4 ± 2.8
LC4		0.20	2.5	198.10 ± 8.00	0.233 ± 0.028	+33.4 ± 3.6
LC5		0.20	3.0	185.10 ± 14.50	0.269 ± 0.031	+31.6 ± 3.8
LC6		0.20	3.5	461.20 ± 26.10	0.640 ± 0.051	+25.5 ± 2.4

Table 2
Effect of chitosan concentration, molecular weight and SBE-β-CD concentration on the drug content (DC), loading capacity (LC), actual yield and yield percentage for the prepared nanoparticles (mean ± SD).

Formula code	DC (%)	LC (%)	Actual yield (g)	Yield (%)
HC1	13.37 ± 0.61	0.58 ± 0.03	0.58 ± 0.02	36.25 ± 1.25
HC2	14.21 ± 0.10	0.47 ± 0.02	0.76 ± 0.03	35.23 ± 1.39
LC1	23.97 ± 1.32	14.71 ± 0.81	0.41 ± 0.02	25.47 ± 1.24
LC2	30.23 ± 1.09	15.95 ± 0.58	0.47 ± 0.03	22.03 ± 1.41
LC3	41.51 ± 2.79	15.09 ± 1.01	0.69 ± 0.05	25.94 ± 1.88
LC4	35.41 ± 5.06	1.94 ± 0.28	0.79 ± 0.07	29.29 ± 2.30
LC5	43.95 ± 6.06	9.72 ± 1.34	1.15 ± 0.04	36.02 ± 1.25
LC6	45.67 ± 1.33	8.33 ± 0.24	1.37 ± 0.12	37.03 ± 3.24

Table 3
Effect of drug concentration on the particle diameter, polydispersity index (PDI), zeta potential, drug content (DC) and loading capacity (LC) (mean ± SD).

Formula code	Particle diameter (nm)	PDI	Zeta potential (mV)	DC (%)	LC (%)
LC3	182.3 ± 18.3	0.353 ± 0.020	+25.4 ± 2.8	41.51 ± 2.79	15.09 ± 1.01
LC3-2	217.6 ± 10.5	0.408 ± 0.022	+25.1 ± 2.4	45.32 ± 2.75	32.96 ± 2.00
LC3-3	104.8 ± 18.1	0.205 ± 0.025	+23.0 ± 2.5	29.91 ± 0.93	35.60 ± 1.11
LC5	185.1 ± 12.5	0.269 ± 0.026	+31.6 ± 3.8	43.95 ± 6.06	9.72 ± 1.34
LC5-2	143.3 ± 11.3	0.240 ± 0.031	+29.4 ± 3.0	35.54 ± 2.34	15.41 ± 1.01
LC5-3	158.8 ± 13.0	0.263 ± 0.029	+27.3 ± 3.0	27.52 ± 2.20	17.90 ± 1.43
LC6	461.2 ± 14.5	0.640 ± 0.031	+25.5 ± 2.4	45.67 ± 1.33	8.33 ± 0.24
LC6-2	673.1 ± 26.1	0.716 ± 0.028	+22.3 ± 2.1	29.72 ± 2.45	10.85 ± 0.89
LC6-3	132.4 ± 8.2	0.280 ± 0.051	+23.1 ± 2.8	39.15 ± 3.01	21.43 ± 1.65

The formulations LC3, LC3-2 and LC5 showed smaller particle diameter (182.3, 217.6 and 185.1 nm, respectively), lower PDI (0.353, 0.408 and 0.269, respectively), highest zeta potential (25.4, 25.1 and 31.6, respectively) and higher drug content (41.51, 45.32 and 43.95, respectively) were chosen for further studies.

3.2.3. Nanoparticles morphology

The TEM image (Fig. 3) indicated that CS/SBE-β-CD nanoparticles were predominantly spherical in shape with an irregular surface. The diameter of the nanoparticles based on the TEM micrographs was about 90–150 nm smaller than the diameter determined by photon correlation spectroscopy. This could have been expected since the nanoparticles were dispersed in an aqueous phase for the photon correlation spectroscopy experiments, and CS has the ability to swell in contact with water, while the TEM experiments were performed in dry samples (Aktas et al., 2005).

3.2.4. In vitro release studies

The results of the drug release experiments from the three optimized CS/SBE-β-CD nanoparticles and drug solution in phosphate buffer pH 7.4 are shown in Fig. 4. ECO solution showed a fast release profile with 100% ECO released within 1 h. All the tested formulations displayed similar controlled release profiles (f_2 values 73–80) following zero-order release model with about 50% of the ECO was released in 8 h. The retardant effect of CS can be explained by the slow diffusion of ECO through the more hydrophilic CS/CD matrix layer around the lipophilic drug (Cerchiara et al., 2003).

Nanoparticles LC3 showed a lag time (about 1 h) in drug release that was not evident in the corresponding formulation LC3-2 containing the same composition but with higher drug loading capacity. This could indicate that LC3 had more compact solid matrix structure compared to that of LC3-2. This is in agreement with the fact that drug loading capacity is an important factor for the release property of nanoparticles. Since higher drug loading

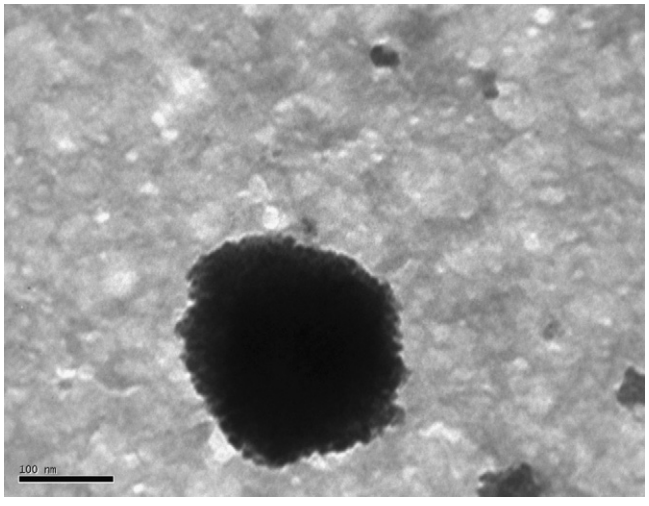

Fig. 3. Transmission electron micrograph of the ECO-loaded CS/SBE-β-CD nanoparticles.

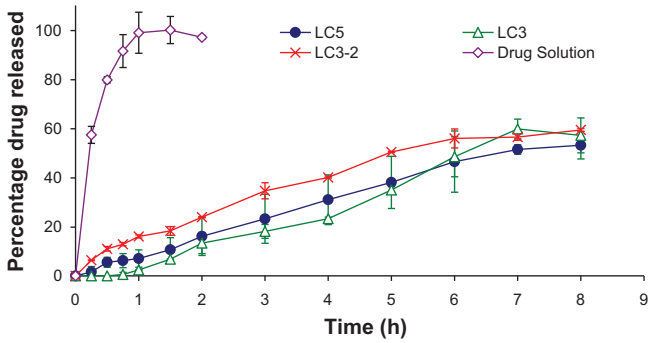

Fig. 4. *In vitro* release profiles of the CS/SBE-β-CD optimized nanoparticles formulations and drug solution in phosphate buffer pH 7.4.

capacity leads to a wider concentration gap between the polymeric nanospheres and the release medium, and causes a higher drug release rate (Xu and Du, 2003). LC3-2 and LC5 with similar drug release profiles were chosen for further investigations.

3.2.5. Fourier transform infrared spectroscopy (FT-IR)

ECO, CS, SBE-β-CD, their physical mixture and ECO loaded nanoparticles (LC3-2 and LC5) were analysed using FT-IR spectrophotometer for characteristic absorption bands (Fig. 5). The IR spectrum of ECO showed evident several characteristics peaks: aromatic C–H stretching vibrations at 3174 and 3107 cm^{-1}; aromatic C=C and C=N stretching vibrations at 1587 and 1548 cm^{-1}; aromatic C–Cl stretching vibrations at 1219 cm^{-1}; C–O–C stretching vibrations at 1087 cm^{-1}. In the CS spectrum the strong peak at 3416 cm^{-1} corresponds to combined peaks of O–H stretching and intermolecular hydrogen bonding. The N–H stretching from primary amines is overlapped in the same region. The symmetric stretch of C–O–C is found around 1078 cm^{-1}, and the intense peak at 1422 cm^{-1} belongs to the C–N stretching. The N–H bending peak at 1597 cm^{-1} and the band for amide I at 1657 cm^{-1} are seen in the

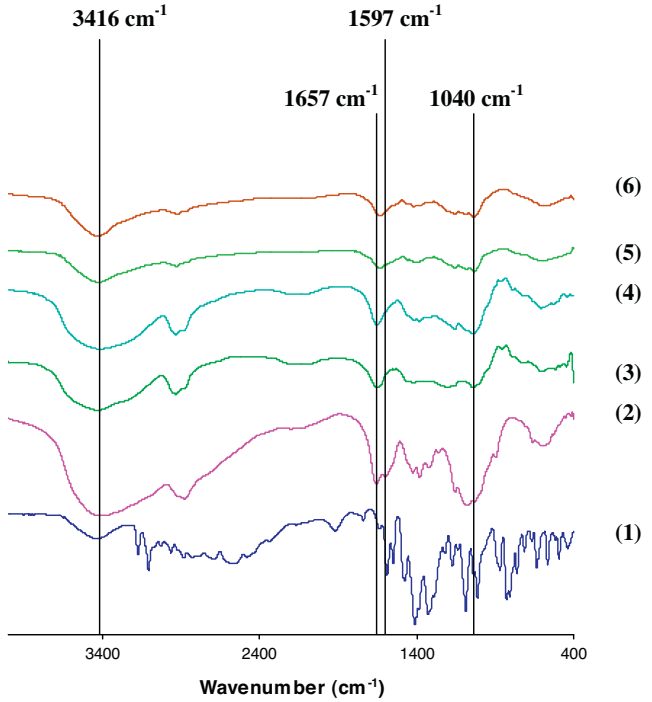

Fig. 5. FT-IR spectra of (1) ECO, (2) CS, (3) SBE-β-CD, (4) physical mixture of ECO, CS and SBE-β-CD, (5) LC3-2 nanoparticles and (6) LC5 nanoparticles.

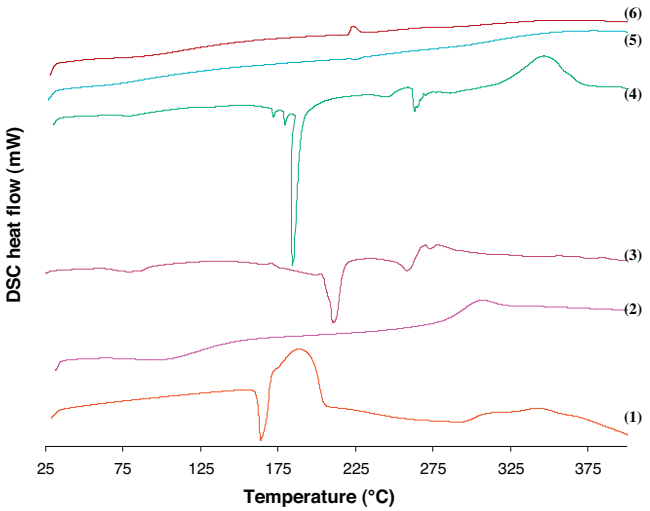

Fig. 6. Thermograms of (1) ECO, (2) CS, (3) SBE-β-CD, (4) physical mixture of ECO, CS and SBE-β-CD, (5) LC3-2 nanoparticles and (6) LC5 nanoparticles.

IR spectrum of CS. The IR spectrum of SBE-β-CD is characterized by intense bands at 3300–3500 cm^{-1} due to O–H stretching vibrations and a sulfoxide stretch at 1040 cm^{-1}. The vibration of the –CH and CH_2 groups appears in the 2800–3000 cm^{-1} region.

The spectrum patterns of the physical mixtures corresponded simply to superposition of the IR spectra of chitosan and SBE-β-CD. The characteristics peaks for ECO were almost completely obscured by the very intense and broad peaks of chitosan and SBE-β-CD because of the small proportion of ECO in the physical mixture and the investigated nanoparticles. This makes the use of infrared spectroscopy as an insignificant method to detect interaction between ECO and SBE-β-CD.

The FT-IR spectrum of ECO loaded CS/SBE-β-CD nanoparticles LC3-2 and LC5 are different from that of CS matrix. In LC3-2 and LC5 nanoparticles the tip of the peak at 3416 cm^{-1} was shifted to 3428 cm^{-1} indicating that hydrogen bonding is enhanced. The 1597 cm^{-1} peak of N–H bending vibration disappeared and the peak at 1657 cm^{-1} was shifted to 1630 and 1629 cm^{-1} for LC3-2 and LC5 nanoparticles, respectively. The sulfoxide stretch at 1040 cm^{-1} for SBE-β-CD was shifted to 1036 cm^{-1} for LC3-2 and LC5 nanoparticles. These spectral changes could be attributed to the electrostatic interaction between CS cationic amine and SBE-β-CD anionic sulfobutyl groups (Tiyaboonchai and Limpeanchob, 2007).

3.2.6. Differential scanning calorimetry (DSC)

The DSC profiles of pure components, their corresponding physical mixture and ECO loaded nanoparticles (LC3-2 and LC5) are presented in Fig. 6. ECO exhibited a sharp endothermic peak at 164 °C followed by a large, irregular exothermic peak. CS showed characteristic endothermic peak at 93 °C and an exothermic peak at 306 °C. SBE-β-CD showed a broad endothermic peak at about 67 °C corresponding to the liberation of crystal water, whereas those at higher temperatures (at 212 and 258 °C) were due to sample decomposition. Thermogram of physical mixture showed a sharp endothermic peak at 183 °C, which probably represents the coalescence of both isolated endothermic peaks of ECO and SBE-β-CD. In addition, an endothermic and exothermic peaks at 261 and 346 °C, respectively, resulted from individual contribution of SBE-β-CD and CS, respectively. The characteristic peak for ECO was found to disappear and could not be seen in ECO loaded nanoparticles, indicating the amorphous dispersion of ECO in CS nanoparticles.

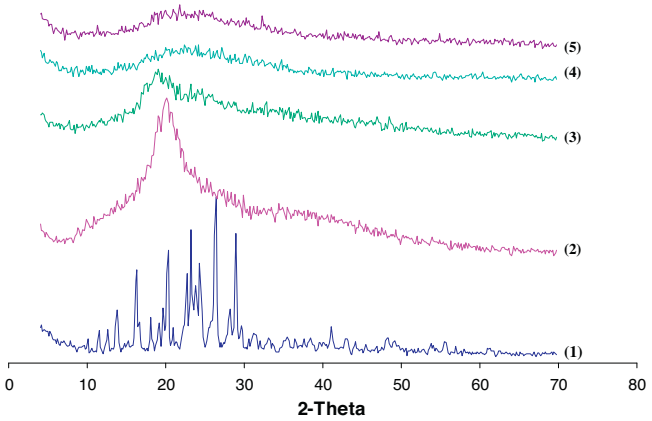

Fig. 7. X-ray diffraction of (1) ECO, (2) CS, (3) SBE-β-CD, (4) LC3-2 nanoparticles and (5) LC5 nanoparticles.

3.2.7. X-ray diffractometry

Fig. 7 shows the X-ray diffraction pattern of ECO, CS, SBE-β-CD, their corresponding physical mixture and ECO loaded nanoparticles (LC3-2 and LC5). ECO has specific sharp crystal peaks and CS has a specific broad peak, while a halo-pattern was recorded for SBE-β-CD demonstrating their amorphous states. When ECO was encapsulated into CS nanoparticles, its sharp crystal peaks were overlapped with the noise of the coated polymer and disappeared, indicating that ECO was completely and successfully encapsulated into core of CS nanoparticles.

3.2.8. Mucoadhesion studies

The influence of the mucin on the zeta potential of the tested nanoparticles revealed a reduction in the zeta potential values for CS nanoparticles occurring on mixing with mucin (Fig. 8). This reduction could be attributed to the ionic interaction between negatively charged sialic acid residues in mucin and positively charged amino groups in CS nanoparticles that resulted in the mucoadhesive properties of the tested CS nanoparticles. This unique property makes the prepared nanoparticles a versatile delivery system which fulfils the requirements for application in the ophthalmic field. LC5 nanoparticles showed more reduction in zeta potential value on mixing with mucin indicating more mucoadhesive properties compared to that of LC3-2. This may be attributed to

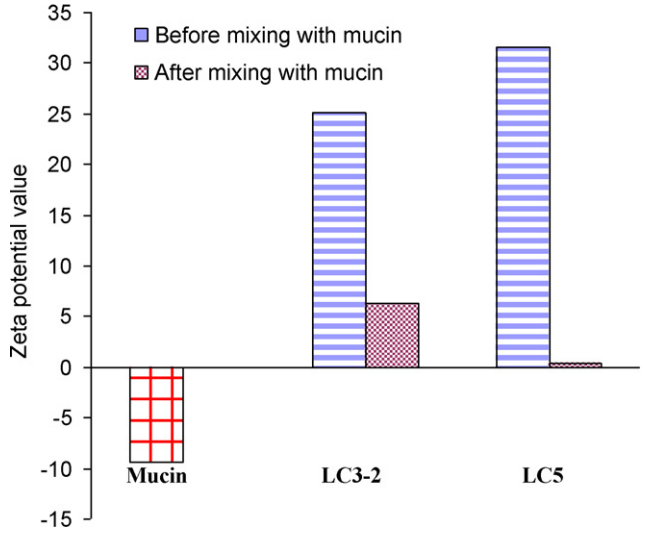

Fig. 8. Zeta potential values obtained for mucin and LC3-2 and LC5 nanoparticles before and after incubation with mucin.

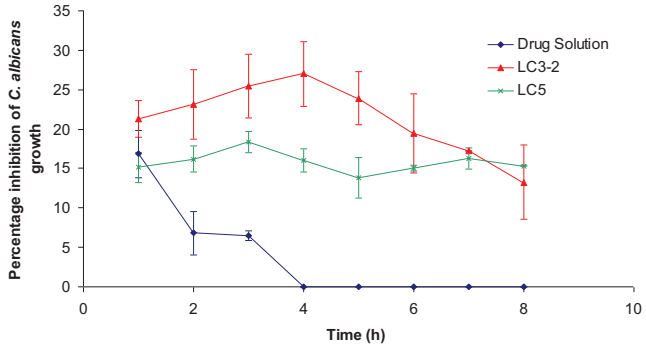

Fig. 9. Percentage inhibition of *C. albicans* growth produced by ECO solution, LC3-2 and LC5 nanoparticles in the external tissues of albino rabbits.

the fact that LC5 nanoparticles had about double the actual yield of nanoparticles compared to that of LC3-2 (Table 3). Thus, more nanoparticles are available to interact with mucin.

3.3. In vivo evaluation of ECO loaded CS nanoparticles

In order to investigate whether or not the nanoparticulate of CS played a role in ocular drug delivery, the antifungal effect of ECO loaded CS/SBE-β-CD nanoparticles was compared to that of ECO solution. Results showed that the tested ECO loaded CS/SBE-β-CD nanoparticles provided, to the eye surface, greater antifungal effect than that of ECO solution (Fig. 9). The differences in ECO effect for the nanoparticles and the solution were significantly higher at all times assayed with the exception of time 1 h ($p < 0.05$). This might be attributed to the mucoadhesive properties of the ECO loaded CS/SBE-β-CD.

The AUC value for LC3-2 was significantly higher ($p < 0.05$) than that for LC5 (170 ± 6 and 127 ± 5, respectively). The ECO antifungal effect associated with the application of LC3-2 nanoparticles increased gradually with time showing a maximum at 4 h post-administration, and then decreased gradually afterwards. In contrast, LC5 nanoparticles showed a fairly constant ECO antifungal effect through the duration of the study. Thus, the *in vivo* test has evidenced a significance difference between the antifungal effect of ECO loaded LC3-2 and LC5 nanoparticles, whereas the *in vitro* release studies were unable to detect any significant difference between the ECO releases of the two nanoparticles formulations. This discrepancy can be explained by considering that in the *in vivo* model the cornea is covered by a mucous layer, which is absent from the *in vitro* release studies. Because the two tested nanoparticles had similar drug concentration values but different in their mucoadhesive properties, and hence, the sustained effect of the LC5 nanoparticles in the *in vivo* model was expected to be stronger than that of LC3-2 nanoparticles. The high mucoadhesive properties of LC5 nanoparticles compared to that of LC3-2 nanoparticles would form a layer of mucin around the LC5 nanoparticles that would promote ECO release and thus promote its effect and retain it for a longer period in the eye compared to LC3-2 nanoparticles.

4. Conclusion

Ionically crosslinked CS/SBE-β-CD nanoparticles represent an interesting CS-based delivery system for hydrophobic drugs to the ocular mucosa. The viscosity of CS and the ratio between CS and SBE-β-CD were critical and controlled the size, zeta potential and drug content of the prepared particles. Furthermore, the drug release from optimized ECO loaded CS/SBE-β-CD nanoparticles showed a sustained drug release manner. CS nanoparticles showed a mucoadhesive properties that enable them to interact

with the ocular mucosa for an extended period of time, thus they provided an enhanced and controlled effect of the drug to ocular surface of rabbits eyes. Consequently, these nanocarriers represented a promising approach for the circumvention of the present limitations in ocular drug delivery.

Acknowledgements

The authors would like to thank the National Research Centre (NRC), Cairo, Egypt for financial support. Our special gratitude to Dr. Alaa H. Salama (Department of Pharmaceutical Technology, NRC) for her suggestions and support.

References

Aachmann, F.L., Otzen, D.E., Larsen, K.L., Wimmer, R., 2003. Structural background of cyclodextrin–protein interactions. Protein Eng. 16, 905–912.

Aktas, Y., Andrieux, K., Alonso, M.J., Calvo, P., Gursoy, R.N., Couvreur, P., Capan, Y., 2005. Preparation and *in vitro* evaluation of chitosan nanoparticles containing a caspase inhibitor. Int. J. Pharm. 298, 378–383.

Al-Marzouqi, A.H., Elwy, H.M., Shehadi, I., Adem, A., 2009. Physicochemical properties of antifungal drug-cyclodextrin complexes prepared by supercritical carbon dioxide and by conventional techniques. J. Pharm. Biomed. Anal. 49, 227–233.

Calvo, P., Remunan-Lopez, C., Vila-Jato, J.L., Alonso, M.J., 1997. Novel hydrophilic chitosan–polyethylene oxide nanoparticles as protein carriers. J. Appl. Polym. Sci. 63, 125–132.

Cerchiara, T., Luppi, B., Bigucci, F., Zecchi, V., 2003. Effect of chitosan on progesterone release from hydroxypropyl-beta-cyclodextrin complexes. Int. J. Pharm. 258, 209–215.

Colonna, C., Conti, B., Perugini, P., Pavanetto, F., Modena, T., Dorati, R., Iadarola, P., Genta, I., 2008. Ex vivo evaluation of prolidase loaded chitosan nanoparticles for the enzyme replacement therapy. Eur. J. Pharm. Biopharm. 70, 58–65.

Csaba, N., Garcia-Fuentes, M., Alonso, M.J., 2006. The performance of nanocarriers for transmucosal drug delivery. Expert Opin. Drug Deliv. 3, 463–478.

Csaba, N., Koping-Hoggard, M., Alonso, M.J., 2009. Ionically crosslinked chitosan/tripolyphosphate nanoparticles for oligonucleotide and plasmid DNA delivery. Int. J. Pharm. 382, 205–214.

Cui, F., Qian, F., Yin, C., 2006. Preparation and characterization of mucoadhesive polymer-coated nanoparticles. Int. J. Pharm. 316, 154–161.

De Campos, A.M., Sanchez, A., Alonso, M.J., 2001. Chitosan nanoparticles: a new vehicle for the improvement of the delivery of drugs to the ocular surface. Application to cyclosporin A. Int. J. Pharm. 224, 159–168.

de la Fuente, M., Ravina, M., Paolicelli, P., Sanchez, A., Seijo, B., Alonso, M.J., 2010. Chitosan-based nanostructures: a delivery platform for ocular therapeutics. Adv. Drug. Deliv. Rev. 62, 100–117.

Kawashima, Y., Yamamoto, H., Takeuchi, H., Kuno, Y., 2000. Mucoadhesive DL-lactide/glycolide copolymer nanoparticles coated with chitosan to improve oral delivery of elcatonin. Pharm. Dev. Technol. 5, 77–85.

Kayser, O., Lemke, A., Hernandez-Trejo, N., 2005. The impact of nanobiotechnology on the development of new drug delivery systems. Curr. Pharm. Biotechnol. 6, 3–5.

Krauland, A.H., Alonso, M.J., 2007. Chitosan/cyclodextrin nanoparticles as macromolecular drug delivery system. Int. J. Pharm. 340, 134–142.

Motwani, S.K., Chopra, S., Talegaonkar, S., Kohli, K., Ahmad, F.J., Khar, R.K., 2008. Chitosan–sodium alginate nanoparticles as submicroscopic reservoirs for ocular delivery: formulation, optimisation and *in vitro* characterisation. Eur. J. Pharm. Biopharm. 68, 513–525.

Oyarzun-Ampuero, F.A., Brea, J., Loza, M.I., Torres, D., Alonso, M.J., 2009. Chitosan–hyaluronic acid nanoparticles loaded with heparin for the treatment of asthma. Int. J. Pharm..

Paul, W., Sharma, C.P., 2000. Chitosan, a drug carrier for the 21st century: a review. STP Pharma Sci. 10, 5–22.

Reynolds, J.E.F., 1996. Martindale, The Extra Pharmacopoeia, 31st ed. Royal Pharm. Soc., Pharmaceutical Press, London.

Schiffelers, R.M., Woodle, M.C., Scaria, P., 2004. Pharmaceutical prospects for RNA interference. Pharm. Res. 21, 1–7.

Tiyaboonchai, W., Limpeanchob, N., 2007. Formulation and characterization of amphotericin B–chitosan–dextran sulfate nanoparticles. Int. J. Pharm. 329, 142–149.

U.S. Department of Health and Human Services, 1997. Guidance for Industry: Dissolution Testing of Immediate Release Solid Oral Dosage Forms. Food and Drug Administration Center for Drug Evaluation and Research (CDER).

van der Lubben, I.M., Verhoef, J.C., Borchard, G., Junginger, H.E., 2001. Chitosan for mucosal vaccination. Adv. Drug Deliv. Rev. 52, 139–144.

Vandenberg, G.W., Drolet, C., Scott, S.L., de la Noue, J., 2001. Factors affecting protein release from alginate-chitosan coacervate microcapsules during production and gastric/intestinal simulation. J. Control. Release 77, 297–307.

Xu, Y., Du, Y., 2003. Effect of molecular structure of chitosan on protein delivery properties of chitosan nanoparticles. Int. J. Pharm. 250, 215–226.

Zia, V., Rajewski, R.A., Stella, V.J., 2001. Effect of cyclodextrin charge on complexation of neutral and charged substrates: comparison of (SBE)7M-beta-CD to HP-beta-CD. Pharm. Res. 18, 667–673.